

# High-Throughput, Ultrafast Synthesis of Solution-Dispersed Graphene via a Facile Hydride Chemistry\*\*

Nihar Mohanty, Ashvin Nagaraja, Jose Armesto, and Vikas Berry\*

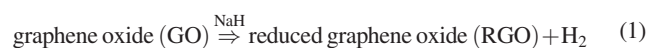
Graphene is a single-atom-thick two-dimensional macromolecule with  $sp^2$ -bound carbon atoms<sup>[1]</sup> arranged in a honeycomb lattice. Recently, graphene has emerged as an attractive candidate for several applications, including ultrafast nanoelectronic devices,<sup>[2,3]</sup> tunable spintronics,<sup>[4]</sup> ultracapacitors,<sup>[5]</sup> transparent conducting electrodes,<sup>[6,7]</sup> single-molecule chemical sensors,<sup>[8]</sup> ultrasensitive biodevices,<sup>[9]</sup> and nanomechanical devices.<sup>[10]</sup> These applications have evolved from its atypical properties, such as weakly scattered ballistic transport of charge carriers behaving as massless fermions at room temperature,<sup>[3,11]</sup> magneto-sensitive transport,<sup>[12–14]</sup> tunable bandgap,<sup>[15]</sup> quantum Hall effect at room temperature,<sup>[12–14]</sup> tunable optical transitions,<sup>[16,17]</sup> exceptional mechanical strength,<sup>[18]</sup> megahertz characteristic frequency,<sup>[10]</sup> carrier collimation, and ultrahigh stiffness.

Graphene can be 1) synthesized on-substrate, 2) deposited on-substrate via mechanical processes, or 3) deposited on-substrate from solution. On-substrate synthesis includes high-temperature (>1000 °C) epitaxial growth on SiC,<sup>[19,20]</sup> ruthenium<sup>[21]</sup> or chemical vapor deposition on nickel<sup>[22]</sup> and copper,<sup>[23]</sup> while mechanical deposition includes adhesive-tape exfoliation of highly oriented pyrolytic graphite (HOPG) and the ensuing transfer. The third process, which is based on on-substrate deposition from a graphene suspension, has several advantages including the large-scale production of reduced graphene oxide (RGO) and easy-to-apply chemical and physical manipulations for functionalization and directed deposition.<sup>[24–28]</sup> Graphene suspension synthesis methods include 1)  $\pi$ - $\pi$  intercalation or graphite intercalation compound (GIC)-based exfoliation of graphite flakes into graphene sheets,<sup>[24,25,29,30]</sup> and 2) in-solution reduction of graphite oxide prepared by Hummers method<sup>[15,31,32]</sup> with hydrazine.<sup>[26–28,33]</sup> The  $\pi$ - $\pi$  intercalation and GIC-based methods produce high-quality graphene; however, the yield is low with relatively low stability of the graphene solution, in which the graphene sheets have a tendency to settle down. The graphene suspension

prepared by in-solution or 180 °C solvothermal reduction of graphene oxide (GO) in hydrazine produces a higher yield and stability; however, the process takes several days for completion.<sup>[34]</sup> Supercritical water has been used for the reduction of GO into graphene, for which high pressures and temperatures are required in a closed system, and the process takes about 6 h for completion.<sup>[35]</sup> Recently, sodium borohydride and concentrated sulfuric acid have been used to reduce GO sheets via a two-step reduction process, which takes about 3 days for completion.<sup>[36,37]</sup>

Herein, we present a novel route to reduce GO and stabilize RGO in dispersions in a methanol suspension using common reagents via an ultrafast (less than a minute), high-throughput, single-step process. Sodium hydride acts both as a reducing agent to reduce GO to RGO and as a deprotonator to convert methanol to methoxy ions. These methoxy ions then stabilize the RGO sheets in the bulk methanol. Multilayer RGO sheets as large as >10 000  $\mu\text{m}^2$  with high  $sp^2$  to  $sp^3$  ratio and low defect density were obtained with conductivities of  $\approx 4500$ – $10\,625\text{ S m}^{-1}$  with electron and hole mobilities of 100–400 and 300–600  $\text{cm}^2\text{ V}^{-1}\text{ S}^{-1}$ , respectively. These values are comparable with the highest values reported for multilayer RGO.<sup>[38]</sup>

GO sheets suspended in water were synthesized from mesh 7 graphite flakes (Sigma–Aldrich) via a modified Hummers acid oxidation method, which produces one- to four-atom-thick sheets of partially oxidized graphene with the surface containing negatively charged hydroxyl, epoxy, and carboxylic acid groups, which electrostatically stabilize the GO sheets in suspension. The addition of the electronegative oxygen and the removal of unsaturated  $\pi$  electrons cause the GO sheets to be distorted due to the introduction of nonplanar  $sp^3$  bonds (Figure 1, top). The GO suspension samples were centrifuged (11 000 g, 60 min, 20 °C) and resuspended in 99% methanol with intermittent sonication.<sup>[39]</sup> Methanol-dispersed GO was then exposed to pure sodium hydride powder (final concentration  $\approx 100\text{ mg mL}^{-1}$ ), which instantaneously (a few seconds) reduced GO to RGO, while generating hydrogen gas bubbles. Further, sodium hydride deprotonates methanol to methoxy ions,<sup>[40]</sup> which is expected to stabilize the RGO sheets in methanol. Finally, a dark black, highly stable (about one month) solution of RGO was produced. Based on the initial weight of the graphite flakes, the process gave a yield of  $\approx 68\%$  with most RGOs having one to four layers. The yield for the NaH-based GO to RGO reduction process was close to 100%. The chemistry is shown below:<sup>[40]</sup>



[\*] Dr. V. Berry, N. Mohanty, A. Nagaraja, J. Armesto  
Department of Chemical Engineering  
Kansas State University  
1005 Durland Hall, Manhattan, KS 66506 (USA)  
E-mail: vberry@ksu.edu

[\*\*] We thank Dr. Paula Spencer and Dr. Charles Ye for help with Raman characterization. We also thank Myles Ikenbury and Dr. Keith Hohn for help with FTIR spectroscopy. We thank Dr. David Moore and Heather Shinogle for help with FESEM. V.B. thanks NSF (contract CMMI-0939523) and KSU for financial support.

Supporting Information is available on the WWW under <http://www.small-journal.com> or from the author.

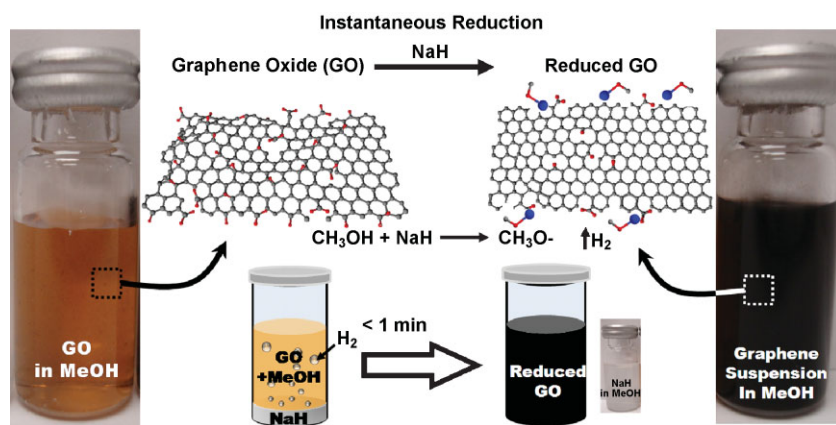


**Figure 1.** Schematic diagram of the hydride reduction process. Photographs of glass vials containing a dispersion of the GO in methanol (left) and a stable dispersion of RGO in bulk methanol (right). Center right, bottom: picture of a vial with NaH in methanol. The dark black color of the stabilized RGO in contrast to the yellow color of the GO indicates the partial restoration of the interlayer  $\pi$  network of the RGO sheets. The cartoon and the three-dimensional (3D) chemical structures (the gray, red, and blue balls denote the carbon, oxygen, and sodium atoms, respectively, in the ball-and-stick model) show the reduction process of GO to RGO via hydride chemistry, the associated release of hydrogen gas, and the ensuing solution stabilization of the RGO by sodium methoxide ions.

The relatively low exothermicity ( $T_{\text{rxn}} < 350 \text{ K}$ ,  $T_{\text{autoignition}} \approx 858 \text{ K}$ ; source: NIST) of the reaction at the experimental volumes reduces the fire hazard from the hydrogen gas produced during the reaction. The RGO suspension was highly stable with no visible settling, which can be attributed to the adsorbed methoxide ion ( $\text{Na}^+\text{CH}_3\text{O}^-$ )-induced electrostatic repulsion between individual RGO sheets in methanol.<sup>[41]</sup>

Field-emission scanning electron microscopy (FESEM) images of the RGO sheets immediately after the hydride reaction show dendritic structures of sodium methoxide deposited on the RGO surface, the chemical composition of which was confirmed by energy-dispersive X-ray (EDX) analysis (see Supporting Information, Figure S1). Addition of deionized (DI) water to the suspension destabilizes the solution resulting in the formation of large clusters, which slowly settle down. This finding can be attributed to the removal of the stabilizing methoxide ions from the RGO surface. EDX studies confirmed complete sodium removal, which also made the RGO surfaces smooth as observed by FESEM (Figure 2b, inset; see Supporting Information, Figure S2). More studies are needed to completely characterize this process. When a 300-nm-thick silicon dioxide substrate is contacted with a RGO solution for 10 min, a large areal RGO coverage is achieved, as observed by

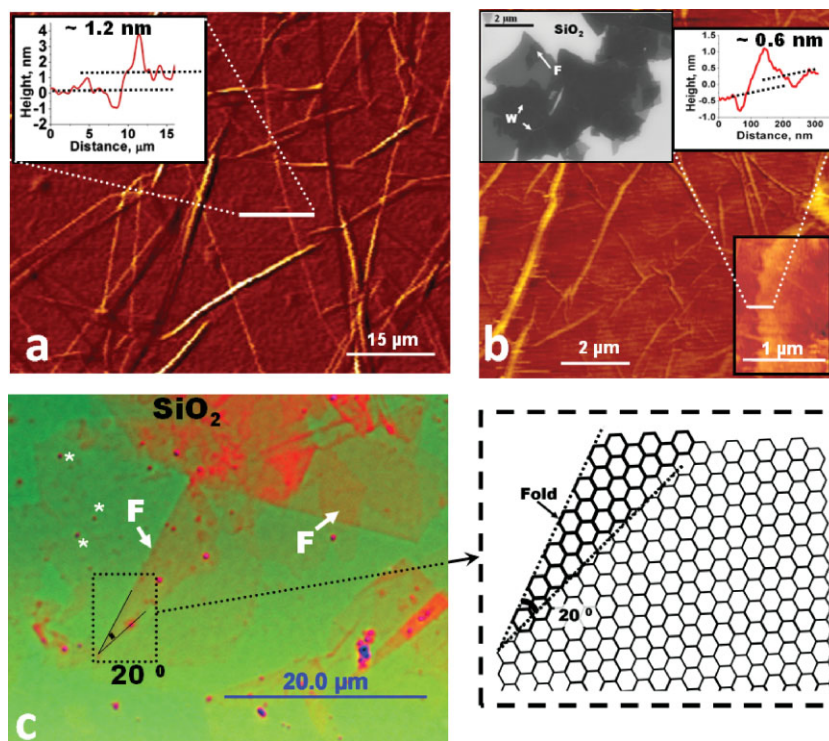


**Figure 2.** a, b) Atomic force microscopy (AFM) images of the GO sheets (a) and RGO sheets (b) spin-coated on 300-nm-thick silica wafers. Insets: the height profiles indicate that the thickness of the GO monolayer is  $\approx 1.2 \text{ nm}$  (a), while that for the RGO monolayer is  $0.6 \text{ nm}$  (top right inset (b)). The top left inset in (b) shows an FESEM image of the washed RGO sheets deposited on a 300-nm-thick silica substrate. The sheets form wrinkles (W) and folds (F). c) Optical image of RGO sheets deposited on a 300-nm-thick silica substrate, which shows large-area coverage of the sporadically folded (F) RGO sheets. The stars indicate the probable residual sodium methoxide deposits on the RGO sheets and on the substrate. The schematic diagram of the carbon structure (right) depicts a possible folding conformation of the RGO sheets on the atomic scale.

FESEM and optical microscopy (Figure 2c; Supporting Information, Figures S2 and S3). AFM studies on deposited GO and RGO sheets showed that RGO has a smaller thickness ( $\approx 0.6 \text{ nm}$ ) than the parent GO, which is higher than the theoretical thickness, also reported by other groups (Figure 2a,b; Supporting Information, Figure S4).<sup>[38]</sup> This can be attributed to either partially unreduced nonplanar oxy-functional groups, remnant  $\text{sp}^3 \text{ C-C}$  bonds, or gas/solvent molecules trapped between the substrate and the RGO sheets.<sup>[42]</sup> Furthermore, RGO was found to show a large density of folds, which is expected because of  $\pi$ - $\pi$  interaction energy within the sheets. A rough schematic (Figure 2c, right) shows one possible folding mechanism using the angle of fold ( $\approx 20^\circ$ ) shown (Figure 2c, left). The RGO sheets form wrinkles, however the wrinkle density is less than that for GO.<sup>[9]</sup> Moreover, the RGO sheets deposited on a substrate do not agglomerate during deposition. This is attributed to the

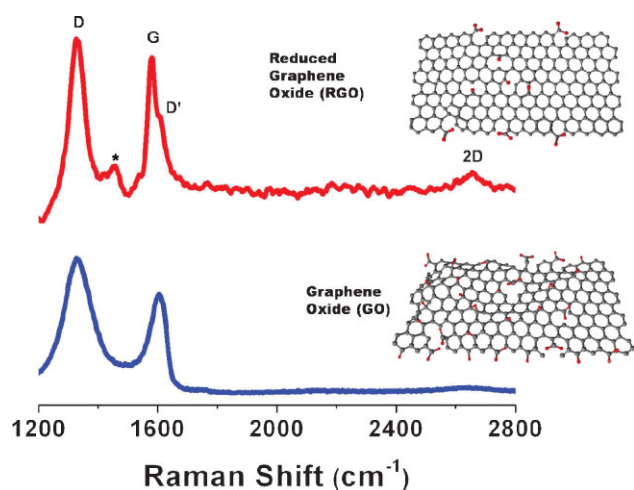


**Figure 3.** Comparison of the Raman spectra of the GO and RGO sheets. The  $I_D/I_G$  and  $I_{D'}/I_G$  ratios for RGO decrease after the reduction process, which suggests the establishment of a long-range crystallographic order of the  $sp^2$  carbon atoms in the RGO structure. The peak marked (\*) in the RGO spectrum can be attributed to residual surface-adsorbed sodium methoxide molecules. The 3D chemical structures on the right depict the GO and RGO sheets.

negatively charged methoxide adsorption on the RGO surfaces, which repel each other.

The RGO sheets were analyzed by Raman (Figure 3), UV/Vis, and Fourier transform infrared (FTIR) spectroscopy (Figure 4) to study the reduction of GO to RGO and to investigate the change in the  $sp^2$  to  $sp^3$  ratio. UV/Vis absorption measurements showed that there was a red shift in the absorbance peak from GO ( $\approx 270$  nm) to RGO (330 nm), which suggests a restoration of the  $\pi$  network of the carbon atoms ( $sp^2$  hybridization) during a reduction of  $sp^3$  to  $sp^2$  bonding (Figure 1). The presence of an absorbance peak at  $\approx 330$  nm compares well with the values reported by other groups (Figure 4b).<sup>[38]</sup> The Raman spectra of the GO and RGO samples were recorded on a spot area of  $\approx 1 \mu\text{m}^2$ , which was far from the sheet edges to avoid signals from the edge defect, and

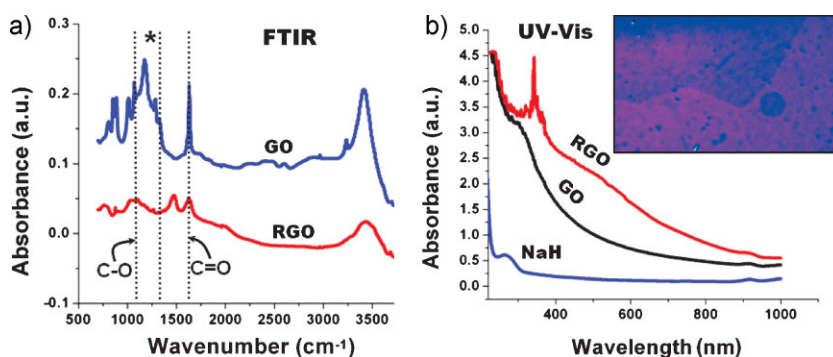


**Figure 4.** a) The FTIR spectra of the RGO and GO samples depict the characteristic peaks for the inherent chemical structure. The starred peak (\*), which corresponds to the fingerprint region for the amorphous carbon, undergoes a sharp decrease in intensity after reduction of GO to RGO, which implies an increased crystallinity of RGO. b) The UV/Vis spectra of RGO, GO, and NaH exhibit the characteristic red shift for RGO, which indicates the restoration of the  $\pi$ -electron network (solvent is methanol). Inset: optical image of a monolayer of RGO spin-coated on a 300-nm-thick silica substrate.

at a low power of  $\approx 5$  mW to reduce localized heating (Figure 3). The Raman peaks at  $\approx 1355 \text{ cm}^{-1}$  (D band) and at  $\approx 1590 \text{ cm}^{-1}$  (G band) agree well with the literature.<sup>[15,33,43]</sup> The slight increase in the position of the G peak compared to that for pristine graphene can be attributed to the remnant n-doping in RGO.<sup>[44,45]</sup>

The  $I_D/I_G$  ratios, which quantify the relative content of the intervalley scattering producing defects (D peak) and the graphenic region (G peak), were calculated from the spectra after baseline correction and integration. While the  $I_D/I_G$  ratio for GO was found to be  $\approx 1.88 \pm 0.25$ , as expected for GO, the  $I_D/I_G$  ratio for RGO was  $\approx 1.08 \pm 0.15$ , which implies a substantial hydride-induced reduction in the relative content of the  $sp^3$  carbon atoms and the oxidized molecular defects, vacancies, etc. (see Supporting Information, Figure S5). This lower value of  $I_D/I_G$  is comparable to that achieved by the supercritical-water-based reduction process ( $I_D/I_G \approx 0.9$ ) and to the recently reported  $180^\circ\text{C}$  solvothermal reduction process ( $I_D/I_G \approx 0.9$ ), and can be attributed to the mild, low exothermic nature of the reduction process. In contrast, the hydrazine reduction of GO<sup>[46]</sup> exhibits an  $I_D/I_G$  ratio of 1.44. Furthermore, the  $I_{D'}/I_G$  ratio, which quantifies the ratio of the weak defects, induced intravalley scattering (D' peak) and the graphenic region (G peak) also decreased after reduction to RGO (see Supporting Information, Figure S5). Using the empirical Tuinstra–Koenig relation, which relates the  $I_D/I_G$  ratio to the crystallite size of the carbonaceous graphitic samples, the size of the ordered graphitic regions in GO was calculated to be  $\approx 4 \text{ nm}^2$ , as expected for a large areal density of  $sp^3$  carbon atoms and defects.<sup>[47]</sup> For RGO, the areal crystallite density with defect-free segments of  $sp^2$  carbon atoms increased threefold and corresponded to a domain size of  $\approx 12.25 \text{ nm}^2$ . The presence of the D/D' band on the entire RGO can be attributed to vacancy defects from the loss of the carbon atoms due to the reduction of the highly oxidized carbon atoms on the parent GO.<sup>[48]</sup> Furthermore, the relatively weak 2D band intensity in RGO spectra can be attributed to the fractional non- $sp^2$  carbon domains, in contrast to the solely  $sp^2$  carbon atoms in the pristine graphene.<sup>[49]</sup>

FTIR studies were conducted to illustrate the chemical structure of the RGO sheets. The RGO and GO sheets were dried in an inert atmosphere (99.9% He,  $200^\circ\text{C}$ ) to obtain powders for characterization. The spectrum for GO agrees well with the values reported in the literature.<sup>[50]</sup> The absorbance peak for GO at  $\approx 1375 \text{ cm}^{-1}$  (appears as a shoulder to the broad peak at  $\approx 1150 \text{ cm}^{-1}$ ), which corresponds to the fingerprint region of amorphous carbon, is greatly reduced in the RGO spectrum, thus signifying the restoration of the honeycomb lattice of carbon atoms. The spectrum for RGO shows a residual peak at  $\approx 1100 \text{ cm}^{-1}$  corresponding to stretching of the C–O bond, which could arise from adsorbed methoxide or defects on the RGO lattice. Furthermore, the intensity of the absorbance peak for GO at  $\approx 1650 \text{ cm}^{-1}$ , which

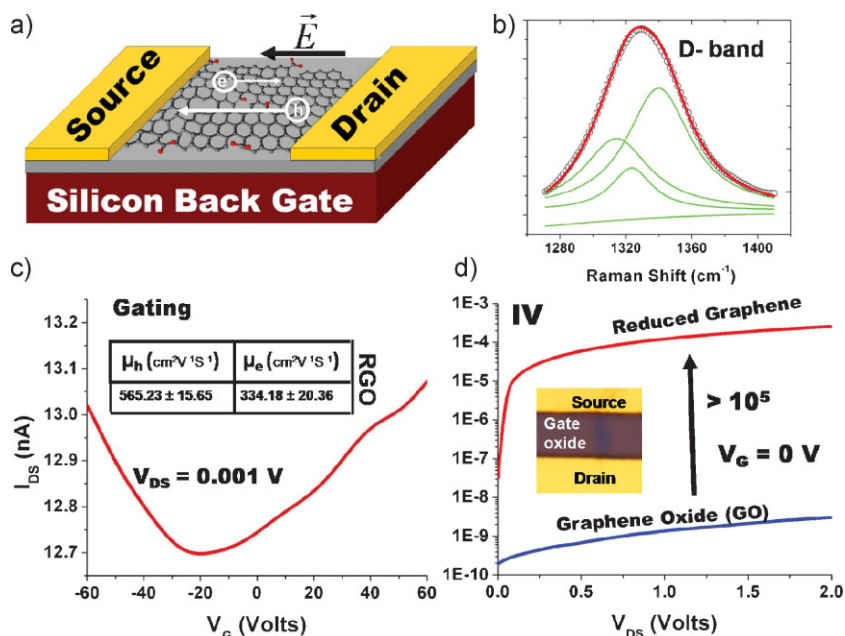


**Figure 5.** a) Schematic diagram of the back-gated field-effect transistor (FET) for studying the electrical properties of RGO.  $\vec{E}$  denotes the electric field; e and h denote electrons and holes, respectively. b) Four-peak Lorentzian fit of the D band from the Raman spectra acquired for the RGO channel in the RGO FET demonstrates a bilayer. c) Electrical gating data for the RGO-based back-gated FET show a slight n-type characteristic. Inset: tabulated values of the calculated carrier mobilities for this RGO bilayer. d) Current–voltage measurements across the source and drain electrodes of a GO sheet, which exhibit a five orders of magnitude increase in conductivity after NaH-induced reduction. Inset: optical image of the RGO FET.

corresponds to stretching of the carbonyl group, reduces by 3.33 in RGO, thus confirming its reduction.

The electrical properties of the thus-produced RGO were studied to determine the charge-carrier properties. RGO sheets were deposited on prepatterned silica (300 nm thermally grown) on n++ silicon substrates with gold electrodes 5  $\mu\text{m}$  apart. The samples were thoroughly washed with DI water and dried in a vacuum. To discern the layer thickness of the RGO channel, the D band from the Raman spectrum acquired earlier (Figure 3) was fitted with the Lorentzian model. A four-peak Lorentzian fit of the D-band-signal curve implied that the sheet was a graphene bilayer<sup>[51]</sup> (Figure 5b; see Supporting Information, Figure S5 for the 2D band fits).<sup>[52]</sup> Similarly, a GO test device was also prepared. The n++ silicon layer was used as a back gate for the field-effect measurements and the 300-nm silica layer functioned as the gate oxide (Figure 5a). The samples were placed in a  $\approx 10^{-4}$  Torr vacuum probe station at room temperature. Figure 5d shows the typical source–drain characteristics of the RGO and GO test devices. The RGO bilayer sheets (prepared by reduction in less than a minute) exhibited conductivities of  $\approx 4500$ – $10\,625 \text{ S m}^{-1}$ , which were five orders of magnitude higher than those of the GO sheets.<sup>[28,38,48]</sup> Furthermore, a GO test device after treatment with sodium hydride solution for 1 min exhibited a three orders of magnitude increase in conductivity, owing to the partial (single side) reduction of GO (Supporting Information, Figure S6).

Electrical gating studies conducted under vacuum showed that the RGO exhibits a slight n-type characteristic, in contrast to the strongly p-type characteristic of the GO sheets.<sup>[9]</sup> The

slight asymmetry in the gating curve (Figure 5) can be attributed to the residual sodium methoxide ions adsorbed on RGO and the charged impurities transferred from the unpassivated silica substrate.<sup>[48,53,54]</sup> Furthermore, upon prolonged washing (6 h) of the as-prepared FET with DI water, near ambipolar carrier density of graphene was restored (see Supporting Information, Figure S7). The electron and hole mobilities for the RGO were computed from the gating data by using the expression:

$$\mu_{\text{carrier}} = (\Delta I_{\text{DS}} / \Delta V_{\text{G}}) / (C_{\text{G}}(l/w) \times V_{\text{DS}}) \quad (3)$$

where  $C_{\text{G}}$  is the silica gate capacitance,  $l$  is the length of the graphene channel, and  $w$  is its width. Owing to the bilayer nature of the RGO channel, the gating effect is expected to be screened by the graphene layers.<sup>[55]</sup> The electron and hole mobilities were calculated to be 100–400 and 300–600  $\text{cm}^2 \text{V}^{-1} \text{S}^{-1}$ , respectively, which are several orders of magnitude higher than those reported for GO.<sup>[55,56]</sup> This further confirms the reduction-induced augmentation of ordered  $\text{sp}^2$  domains (also observed previously in Raman studies), which in turn increases the carrier scattering distance and thus the carrier mobility. Furthermore, the

$I_{\text{DS}}-V_{\text{DS}}$  curves for RGO were found to have nonlinear exponential characteristics (see Supporting Information, Figure S8), which, in conjunction with the limited ordered graphenic domain size ( $\approx 12.25 \text{ nm}^2$ ), suggests a two-dimensional variable-range hopping conduction mechanism, thus vindicating the presence of conducting graphenic domains separated by defects in the RGO sheets.<sup>[26,27,48,57]</sup> However, further studies are needed to characterize this in detail.

In summary, we have demonstrated a novel, ultrafast, and high-yield process to synthesize highly stable RGO dispersions and have illustrated the spectroscopic and electrical characterization of the RGO sheets. The facile hydride chemistry process, which uses commonly available reagents, effectively restores the planar  $\text{sp}^2$ -hybridized structure of graphene, with relatively low defects confirmed by Raman and UV/Vis spectroscopy. The high carrier mobility and the bipolar carrier density in RGO further confirm the increased crystalline  $\text{sp}^2$  regions in RGO with lower scattering distances. These results suggest that this process can a) enable improved handling of graphene dispersions, b) deliver high-quality graphene on demand for electronic, mechanical, and other applications, and c) develop next-generation solution-based graphene functionalization schemes.

## Experimental Section

**Methods for RGO production:** GO sheets suspended in DI water were synthesized from mesh 7 graphite flakes (Sigma–Aldrich) via the modified Hummers acid oxidation method, which

produced one- to four-atom-thick sheets of partially oxidized graphene. The surfaces had negatively charged hydroxyl, epoxy, and carboxylic acid groups, which gave them electrostatic stability in suspension. The GO suspension samples were first spun down using a high-speed centrifugation process (11 000 *g*, 60 min, 20 °C) and subsequently resuspended in anhydrous methanol by intermittent sonication and vortexing. The GO dispersion in methanol was subsequently treated with a fresh sodium hydride (Sigma–Aldrich) powder (100 mg mL<sup>-1</sup>) to instantaneously (less than a minute) reduce GO to RGO. This process turned the yellow GO solution dark black. This solution was left undisturbed for 10 min, followed by high-speed centrifugation at 11 000 *g* for 60 min at 20 °C and washing of the product with DI water five times to remove the sodium methoxide deposits on the RGO sheet surface. Finally, the RGO with adsorbed NaOCH<sub>3</sub> was resuspended in pure methanol to produce a stable RGO dispersion.

**Instruments:** Bright-field optical microscopy imaging was carried out on an Olympus BX40 microscope. FESEM imaging was carried out on a Leo 1550 scanning electron microscope under ultrahigh-vacuum conditions at 10 kV electron high tension (EHT) with a working distance of 4 mm using the Everhart–Thornley detector. AFM studies were carried out at room temperature in a Nanosurf EasyScan 2 microscope with aluminum-coated, highly doped, monolithic silicon-based tapping mode probes (AppNano Inc.). Raman spectra of the samples were collected on a Horiba Jobin Yvon LabRAM ARAMIS Raman spectrometer with a red He–Ne laser ( $\lambda = 632.8$  nm, laser power < 5 mW, spot size  $\approx 1 \mu\text{m}^2$ ), which was parked well away from the sheet's edges to avoid edge effects, a 200-mm confocal pinhole, 150-mm-wide entrance slit, 600 gr mm<sup>-1</sup> grating, and 100 $\times$  objective Olympus lens. FTIR analysis of the samples was carried out on a Newport Oriel MIR8025 FTIR spectrometer. UV/Vis spectroscopic analysis was conducted on a Cole–Parmer scanning UV/Vis spectrophotometer. Electrical characterization of the samples was carried out inside a Janis ST-100 optical cryostat (10<sup>-5</sup> Torr, 300 K) with a Keithley 2612 dual-channel current–voltage source meter.

## Keywords:

graphene · hydrides · multilayers · reduced graphene oxide · synthetic methods

- [1] A. K. Geim, K. S. Novoselov, *Nat. Mater.* **2007**, *6*, 183–191.
- [2] K. S. Novoselov, D. Jiang, F. Schedin, T. J. Booth, V. V. Khotkevich, S. V. Morozov, A. K. Geim, *Proc. Natl. Acad. Sci. USA* **2005**, *102*, 10451–10453.
- [3] K. S. Novoselov, A. K. Geim, S. V. Morozov, D. Jiang, M. I. Katsnelson, I. V. Grigorieva, S. V. Dubonos, A. A. Firsov, *Nature* **2005**, *438*, 197–200.
- [4] D. A. Abanin, P. A. Lee, L. S. Levitov, *Solid State Commun.* **2007**, *143*, 77–85.
- [5] M. D. Stoller, S. Park, Y. Zhu, J. An, R. S. Ruoff, *Nano Lett.* **2008**, *8*, 3498–3502.
- [6] X. Wang, L. J. Zhi, N. Tsao, Z. Tomovic, J. L. Li, K. Mullen, *Angew. Chem.* **2008**, *120*, 3032–3034; *Angew. Chem. Int. Ed.* **2008**, *47*, 2990–2992.
- [7] X. Wang, L. J. Zhi, K. Mullen, *Nano Lett.* **2008**, *8*, 323–327.
- [8] F. Schedin, A. K. Geim, S. V. Morozov, E. W. Hill, P. Blake, M. I. Katsnelson, K. S. Novoselov, *Nat. Mater.* **2007**, *6*, 652–655.
- [9] N. Mohanty, V. Berry, *Nano Lett.* **2008**, *8*, 4469–4476.
- [10] J. S. Bunch, A. M. van der Zande, S. S. Verbridge, I. W. Frank, D. M. Tanenbaum, J. M. Parpia, H. G. Craighead, P. L. McEuen, *Science* **2007**, *315*, 490–493.
- [11] K. S. Novoselov, A. K. Geim, S. V. Morozov, D. Jiang, Y. Zhang, S. V. Dubonos, I. V. Grigorieva, A. A. Firsov, *Science* **2004**, *306*, 666–669.
- [12] D. A. Abanin, K. S. Novoselov, U. Zeitler, P. A. Lee, A. K. Geim, L. S. Levitov, *Phys. Rev. Lett.* **2007**, *98*, 196806.
- [13] K. S. Novoselov, Z. Jiang, Y. Zhang, S. V. Morozov, H. L. Stormer, U. Zeitler, J. C. Maan, G. S. Boebinger, P. Kim, A. K. Geim, *Science* **2007**, *315*, 1379.
- [14] K. S. Novoselov, E. McCann, S. V. Morozov, V. I. Fal'ko, M. I. Katsnelson, U. Zeitler, D. Jiang, F. Schedin, A. K. Geim, *Nat. Phys.* **2006**, *2*, 177–180.
- [15] S. Stankovich, D. A. Dikin, R. D. Piner, K. A. Kohlhaas, A. Kleinhammes, Y. Jia, Y. Wu, S. T. Nguyen, R. S. Ruoff, *Carbon* **2007**, *45*, 1558–1565.
- [16] P. Blake, E. W. Hill, A. H. C. Neto, K. S. Novoselov, D. Jiang, R. Yang, T. J. Booth, A. K. Geim, *Appl. Phys. Lett.* **2007**, *91*, 063124.
- [17] Y. C. Huang, C. P. Chang, M. F. Lin, *Nanotechnology* **2007**, *18*, 495401.
- [18] C. Lee, X. D. Wei, J. W. Kysar, J. Hone, *Science* **2008**, *321*, 385–388.
- [19] C. Berger, Z. M. Song, X. B. Li, X. S. Wu, N. Brown, C. Naud, D. Mayo, T. B. Li, J. Hass, A. N. Marchenkov, E. H. Conrad, P. N. First, W. A. de Heer, *Science* **2006**, *312*, 1191–1196.
- [20] K. V. Emtsev, A. Bostwick, K. Horn, J. Jobst, G. L. Kellogg, L. Ley, J. L. McChesney, T. Ohta, S. A. Reshanov, J. Rohrl, E. Rotenberg, A. K. Schmid, D. Waldmann, H. B. Weber, T. Seyller, *Nat. Mater.* **2009**, *8*, 203–207.
- [21] P. W. Sutter, J. I. Flege, E. A. Sutter, *Nat. Mater.* **2008**, *7*, 406–411.
- [22] K. S. Kim, Y. Zhao, H. Jang, S. Y. Lee, J. M. Kim, K. S. Kim, J. H. Ahn, P. Kim, J. Y. Choi, B. H. Hong, *Nature* **2009**, *457*, 706–710.
- [23] X. Li, W. Cai, J. An, S. Kim, J. Nah, D. Yang, R. Piner, A. Velamakanni, I. Jung, E. Tutuc, *Science* **2009**, 1171245v1.
- [24] X. Li, G. Zhang, X. Bai, X. Sun, X. Wang, E. Wang, H. Dai, *Nat. Nanotechnol.* **2008**, *3*, 538–542.
- [25] Y. Hernandez, V. Nicolosi, M. Lotya, F. M. Blighe, Z. Y. Sun, S. De, I. T. McGovern, B. Holland, M. Byrne, Y. K. Gun'ko, J. J. Boland, P. Niraj, G. Duesberg, S. Krishnamurthy, R. Goodhue, J. Hutchison, V. Scardaci, A. C. Ferrari, J. N. Coleman, *Nat. Nanotechnol.* **2008**, *3*, 563–568.
- [26] S. Gilje, S. Han, M. Wang, K. L. Wang, R. B. Kaner, *Nano Lett.* **2007**, *7*, 3394–3398.
- [27] A. B. Kaiser, C. Gomez-Navarro, R. S. Sundaram, M. Burghard, K. Kern, *Nano Lett.* **2009**, *9*, 1787–1792.
- [28] Y. Si, E. T. Samulski, *Nano Lett.* **2008**, *8*, 1679–1682.
- [29] C. Valles, C. Drummond, H. Saadaoui, C. A. Furtado, M. He, O. Roubeau, L. Ortolani, M. Monthieux, A. Penicaud, *J. Am. Chem. Soc.* **2008**, *130*, 15802–15804.
- [30] J. H. Lee, D. W. Shin, V. G. Makotchenko, A. S. Nazarov, V. E. Fedorov, Y. H. Kim, J. Y. Choi, J. M. Kim, J. B. Yoo, *Adv. Mater.* **2009**, *21*, 1–5.
- [31] W. S. Hummers, R. E. Offeman, *J. Am. Chem. Soc.* **1958**, *80*, 1339.
- [32] Z. Luo, Y. Lu, L. A. Somers, A. T. C. Johnson, *J. Am. Chem. Soc.* **2009**, *131*, 898–8899.
- [33] C. Gomez-Navarro, R. T. Weitz, A. M. Bittner, M. Scolari, A. Mews, M. Burghard, K. Kern, *Nano Lett.* **2007**, *7*, 3499–3503.
- [34] H. Wang, J. T. Robinson, X. Li, H. Dai, *J. Am. Chem. Soc.* **2009**, *131*, 666–669.
- [35] Y. Zhou, Q. Bao, L. A. L. Tang, Y. Zhong, K. P. Loh, *Chem. Mater.* **2009**, *21*, 2950–2956.
- [36] A. B. Bourlinos, D. Gournis, D. Petridis, T. Szabo, A. Szeri, I. Dekany, *Langmuir* **2003**, *19*, 6050–6055.
- [37] W. Gao, L. B. Alemany, L. Ci, P. M. Ajayan, *Nat. Chem.* **2009**, *1*, 403–408.
- [38] D. Li, M. B. Muller, S. Gilje, R. B. Kaner, G. G. Wallace, *Nat. Nanotechnol.* **2008**, *3*, 101–105.

- [39] J. I. Paredes, S. Villar-Rodil, A. Martiñúñez-Alonso, J. M. D. Tascoñin, *Langmuir* **2008**, *24*, 10560–10564.
- [40] H. C. Brown, S. Krishnamurthy, *Tetrahedron* **1979**, *35*, 567–607.
- [41] H. Chen, M. B. Muller, K. J. Gilmore, G. G. Wallace, D. Li, *Adv. Mater.* **2008**, *20*, 3557–3561.
- [42] M. Ishigami, J. H. Chen, W. G. Cullen, M. S. Fuhrer, E. D. Williams, *Nano Lett.* **2007**, *7*, 1643–1648.
- [43] K. N. Kudin, B. Ozbas, H. C. Schniepp, R. K. Prud'homme, I. A. Aksay, R. Car, *Nano Lett.* **2008**, *8*, 36–41.
- [44] A. C. Ferrari, J. C. Meyer, V. Scardaci, C. Casiraghi, M. Lazzeri, F. Mauri, S. Piscanec, D. Jiang, K. S. Novoselov, S. Roth, A. K. Geim, *Phys. Rev. Lett.* **2006**, *97*, 187401.
- [45] C. Casiraghi, S. Pisana, K. S. Novoselov, A. K. Geim, A. C. Ferrari, *Appl. Phys. Lett.* **2007**, *91*, 233108.
- [46] Y. Zhou, Q. Bao, L. A. L. Tang, Y. Zhong, K. P. Loh, *Chem. Mater.* **2009**, *21*, 2950–2956.
- [47] F. Tuinstra, J. L. Koenig, *J. Chem. Phys.* **1970**, *53*, 1126–1130.
- [48] V. C. Tung, M. J. Allen, Y. Yang, R. B. Kaner, *Nat. Nanotechnol.* **2009**, *4*, 25–29.
- [49] L. M. Malard, M. A. Pimenta, G. Dresselhaus, M. S. Dresselhaus, *Phys. Rep.* **2009**, *475*, 51–87.
- [50] T. S. Sreeprasad, A. K. Samal, T. Pradeep, *J. Phys. Chem. C* **2009**, *113*, 1727–1737.
- [51] A. K. Gupta, T. J. Russin, H. R. Gutierrez, P. C. Eklund, *ACS Nano* **2008**, *3*, 45–52.
- [52] A. Gupta, G. Chen, P. Joshi, S. Tadigadapa, P. C. Eklund, *Arxiv preprint cond-mat/0606593* **2006**.
- [53] P. Shemella, S. K. Nayak, *Appl. Phys. Lett.* **2009**, *94*, 032101.
- [54] K. Jasuja, V. Berry, *ACS Nano* **2009**, *3*, 2358–2366.
- [55] A. Reina, X. Jia, J. Ho, D. Nezich, H. Son, V. Bulovic, M. S. Dresselhaus, J. Kong, *Nano Lett.* **2009**, *9*, 30–35.
- [56] G. Gu, S. Nie, R. M. Feenstra, R. P. Devaty, W. J. Choyke, W. K. Chan, M. G. Kane, *Appl. Phys. Lett.* **2007**, *90*, 253507.
- [57] T. Ohta, A. Bostwick, T. Seyller, K. Horn, E. Rotenberg, *Science* **2006**, *313*, 951–954.

Received: August 13, 2009  
 Revised: September 2, 2009  
 Published online: November 26, 2009